Cement 16 (2024) 100098

Contents lists available at ScienceDirect

Cement

journal homepage: www.sciencedirect.com/journal/cement

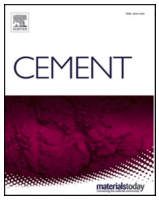

The effect of slag variability in the attempted manufacture of AYF (alite-ye'elimite-ferrite) cement clinker at both laboratory and pilot scale

Visa Isteri [a,*], Katja Ohenoja [b], Christiane Rößler [e], Holger Kletti [e], Pekka Tanskanen [a], Mirja Illikainen [b], Theodore Hanein [c,d], Timo Fabritius [a]

[a] Process metallurgy, Faculty of Technology, University of Oulu, PO Box 4300, 90014 Finland
[b] Fibre and Particle Engineering, Faculty of Technology, University of Oulu, PO Box 4300, 90014 Finland
[c] Manatee Consulting Limited, Sheffield S3 7XL, UK
[d] Department of Materials Science and Engineering, The University of Sheffield, Sheffield S1 3JD, UK
[e] F.A. Finger Institute for Building Materials Science, Bauhaus-University Weimar, Coudraystr. 11, 99421 Weimar, Germany

ARTICLE INFO

Keywords:
Calcium sulphoaluminate cement
Scale-up
Clinkering
Waste valorisation
Alite
Ye'elimite
Mineralisation
AOD slag

ABSTRACT

The production of AYF (alite-ye'elimite-ferrite) clinker was tested at laboratory and semi-industrial scale using by-products from the metallurgical industry: AOD slag; ladle slag; and fayalitic slag. Alite could be produced with ye'elimite using fluorine originating from AOD (argon oxygen decarburisation) slag as a mineraliser. After a successful laboratory demonstration, the clinker production was scaled to a semi-industrial trial. It was discovered that the reason for the absence of alite formation in a semi-industrial demonstration was that the AOD slag from the specific batch did not perform the designed mineralisation effect for alite formation. This study demonstrates that alite-ye'elimite can be produced at 1260 °C at laboratory scale by using fluorine mineralisation originating from an industrial by-product – in this case, AOD slag. However, the utilisation of by-products for delicate reactions requires detailed determination of the properties of the slag, as the variability from the same source yields different clinker chemistries and mineral phases.

1. Introduction

Since the mid-20th century, anthropogenic emissions of greenhouse gases have been amplifying the gas house effect, which causes global warming on Earth [1]. The mitigation strategies for reducing greenhouse gas emissions have forced conventional industry to seek and develop alternative raw materials, products, and ways to improve existing processes.

Portland cement (PC) has been the major binder for the construction industry for the best part of the last two centuries; however, the production of PC includes the calcination of limestone ($CaCO_3$), which is responsible for most of the CO_2 emissions from cement manufacture. The firing process for clinker also produces CO_2 gases through the burning of fossil fuels to reach a sufficient temperature in the kiln [2]. Routes to reduce the CO_2 emissions of cement production include reducing energy/temperature requirements and changing the mineral composition of the PC clinker to fewer calcium-bearing phases and replacing the carbonate rock (limestone) with non-carbonate alternatives.

One approach to achieving these goals is to produce alternative cement clinkers. This study focuses on AYF (alite-ye'elimite-ferrite) chemistry. Adjusting the production temperature of AYF clinker is crucial because the ye'elimite phase decomposes at >1300 °C [3,4], while the typical formation temperature of alite (C_3S) in a conventional rotary kiln is >1350 °C [5]. To close the gap between the formation temperature of alite and ye'elimite, CaF_2 can be used as a mineraliser and flux to ensure the coexistence of these phases [6–8]. With accurate clinker design and an understanding of the chemical and mineralogical composition of the raw materials and an adequate amount of fluoride mineraliser, ye'elimite and alite can be produced at 1250–1260 °C [9–11].

As an alumina source for cement manufacture, bauxite is considered an expensive raw material. To make AYF clinker production more affordable and further reduce the CO_2 emissions of alite-ye'elimite manufacture, it is rational to use alternative raw materials. Studies of the utilisation of industrial by-products for alite-ye'elimite clinkers are

; Cement oxide notation: C, CaO; S, SiO_2; A, Al_2O_3; F, Fe_2O_3; $, SO_3; M, MgO; T, TiO_2.

* Corresponding authors.
E-mail address: visa.isteri@oulu.fi (V. Isteri).

https://doi.org/10.1016/j.cement.2024.100098
Received 8 November 2023; Received in revised form 20 March 2024; Accepted 17 April 2024
Available online 23 April 2024

scarce. Some have been conducted using red mud [12], copper, and phosphorus slag [13] and iron ore (a by-product of the sulfuric acid industry) [11]. The utilisation of AOD (argon oxygen decarburisation) slag and LS (ladle slag) as clinker raw materials has been studied for CSAB clinker [14,15] and PC clinker [16]. No studies of the production of AYF clinker at semi-industrial scale are available.

In this study, the fluorine source for the raw mix was F-bearing AOD slag. For the first time, we assess whether fluorite in AOD slag can be used to replace the CaF_2 mineraliser required to produce alite-ye'elimite clinker. Existing studies of alite-ye'elimite clinkers are conducted at laboratory scale and focus mainly on reagent-grade mineralisers [11, 17–19] and modifying the phase content [9,10,12]. Here, metallurgical slags were used as alternative raw materials in a semi-industrial scale trial to produce AYF clinker. The steelmaking slags used in this study were AOD slag and LS, which are interesting raw material options for AYF clinker because they contain the necessary alumina, calcium, and silicon. Fayalitic slag from nickel production was used for iron source, and phosphogypsum, a residue from fertiliser production, was also used as the $CaSO_4$ source (Adolfsson et al., 2015; Isteri et al., 2020; Iacobescu et al., 2016).

AYF clinker with a target phase composition of 30 wt.% alite, 30 wt. % belite, 30 wt.% ye'elimite, and 10 wt.% ferrite is first synthesised at laboratory scale and then scaled to a semi-industrial scale, in which clinkering is carried out using industrial by-products as raw materials with three different recipes whose fluoride content is adjusted by varying the amount of AOD slag. Detailed microstructural characterisation is performed using XRD and FESEM-EDS on the produced clinkers. The mechanical strength of clinkers with anhydrite addition was also tested through a compressive strength test.

2. Materials and methods

The analyses in this study and sample codes are shown in Table 1. The study was undertaken in three stages. First, a small batch of clinker was made from industrial by-products (AOD slag, ladle slag, and fayalitic slag) in a laboratory furnace (PRE LAB (AOD 1)). The results were then scaled to a semi-industrial kiln, in which three different mixes from similar by-products (PIL A, B, and C) were fired and analysed; however, in the pilot, the AOD slag was from a different batch than in PRE LAB. Because it was found that alite was not formed in the semi-industrial pilot, PRE LAB clinker was remade in a muffle furnace with the same AOD slag batch (AOD 2) as in the semi-industrial trial to confirm the results (this sample is called "POST LAB (AOD 2)"). Additionally, the effect of the particle size of raw materials was tested using ground raw granules from PIL B, which were fired (Ground LAB PIL B) in a muffle furnace and analysed with XRD and EDS.

2.1. Materials

To balance the composition, the reagent-grade chemicals used for the laboratory pre-experiments were calcium carbonate ($CaCO_3$; metal basis, 99.5 %; CAS: 471–34–1), calcium sulphate ($CaSO_4$; anhydrous powder; 99 %; CAS:7778–18–1 and kaolin ($Al_2Si_2O_5(OH)_4$; reagent-grade powder; CAS:1332–58–7).

AOD slag originates from the stainless steelmaking process, in which steel melt is refined in an AOD converter. AOD slag consists of CaO, SiO_2, MgO, and minor amounts of Cr_2O_3 and fluorine [20]. The crystalline phases in AOD slag typically consist of calcium disilicate (Ca_2SiO_4; C_2S) in β (belite) or γ-C_2S (calcio olivine) polymorphs, cuspidine ($Ca_4(Si_2O_7)(F,OH)_2$; $C_4S_2(F,OH)_2$), bredigite ($Ca_7Mg(SiO_4)_4$; C_7MS_4), merwinite ($Ca_3Mg(SiO_4)_2$; C_3MS_2), periclase (MgO; M), fluorite (CaF_2), magnetite (Fe_3O_4; F), free lime (CaO; C), and spinel [20–23]. The major environmental risk of utilising AOD slag is that Cr_2O_3 and F may leech into the environment. In addition, chromium may oxidise to hexavalent chromium, which is carcinogenic [24–26]. Fluorine is added to AOD slag during steelmaking as fluorite (CaF_2) to decrease the viscosity of the slag [27], and chromium originates from chromite ore or scrap metal. The AOD slag for the pilot was analysed by SEM-EDS and XRD analysis, as shown by the results in Appendix 3, to identify the major and fluorine-bearing phases and show the presence of fluorine in the AOD slag.

Ladle slag originates from secondary metallurgy ladle treatment, in which steel melt is refined before casting. The mineralogy of LS in Finland consists of $C_{12}A_7$, γ-C_2S, C_3A, and M, but the phase composition may vary in multiple factors [28]. Fayalitic slag originates from the nickel flash smelting furnace process. The slag is water-granulated, and more than 60 % of it therefore consists of amorphous iron-silicate glass. The crystalline phases are fayalite and magnetite [29]. Phosphogypsum is a by-product from phosphorus fertiliser production [30]. Phosphogypsum is similar to natural gypsum but contains traces of impurities such as P_2O_5 and F^- [30]. Fluorine can be present in phosphogypsum as $Ca_5(PO_4)_3F$. The fluorine content of phosphogypsum could not be detected with X-ray fluorescence (XRF). In previous studies, it was found with ICP (EPA3051A) that 139 ppm of fluorine leeched after a one-stage leeching test, which proves the existence of fluorine. Fayalitic slag is water-granulated and therefore cannot be directly used for clinkering. The grinding of fayalitic slag to pass through a 100 μm sieve is described in Section 2.1.3. Prior to the particle size distribution (PSD) measurement, AOD slag, phosphogypsum, and ladle slag were sieved with a 2 mm sieve and 100 %, 95.5 %, and 86 % passed through respectively. AOD slag, phosphogypsum, and ladle slag were not pre-treated by grinding or sieving for the semi-industrial trial.

In the PRE LAB tests, the industrial by-products used were AOD slag, ladle slag, and fayalitic slag. The XRF analyses of industrial by-products and natural raw materials are presented in Table 2. It should be noted that the AOD slag for the pre-tests (AOD 1) and semi-industrial pilot (AOD 2) was from different batches. AOD slag, fayalitic slag, limestone, and clay were dry materials, but ladle slag (~14 %) and phosphogypsum (~25 %) contained moisture (TG: 125 °C, 1 h). Fayalitic slag was analysed using an Omnian Pananalytics Axiosmax 4 kV spectrometer, and the rest of the raw materials were analysed with a Bruker S8 Tiger. The procedures for XRF and LOI are explained in Section 2.1.4. The LOI of limestone is associated with a loss of CO_2. Fayalitic and AOD slag have a negative LOI due to iron-containing phases that oxidise at higher temperatures.

In the semi-industrial trial, to balance the composition, when necessary, we used Parfill 500 limestone from Nordkalk (Parainen, Finland) and a high alumina-containing clay originating from China. The particle size distributions of the raw materials are presented in Fig. 1. The median particle sizes d_{50} for AOD slag, fayalitic slag, ladle

Table 1
Analyses conducted in this study and sample codes.

Analysis	Raw materials	PRE LAB (AOD 1)	POST LAB (AOD 2)	Granules (ABC)	PIL A	PIL B	PIL C	Ground LAB PIL B
XRD		X	X		X	X	X	X
PSD	X				X	X	X	
XRF	X			X	X	X	X	
TGA	X							
DTA-TG-MS				X				
Density					X	X	X	
SEM + EDS					X	X	X	X

Table 2
Chemical composition of raw materials obtained through the XRF (X-ray fluorescence) analysis and LOI (loss on ignition).

Oxide	Fayalitic slag wt.%	AOD slag 1 wt.%	AOD slag 2 wt.%	Ladle slag wt.%	Limestone wt.%	Phosphogypsum wt.%	Clay wt.%
Al_2O_3	2.9	1.7	1.7	22.9	0.8	0.1	38.7
CaO	2.1	55.4	55.6	37.6	50.5	29.1	0.6
Fe_2O_3	51.3	0.7	0.8	1.6	0.5	0.1	6.1
MgO	6.9	8.7	8.9	6.1	3.1	0.1	0.4
MnO	0.1	0.3	0.3	0.7	0	0	0
Na_2O	0.5	0	0	0.1	0.1	0	0.1
P_2O_5	0	0	0	0	0	0.5	0.1
SiO_2	34.4	28.0	29.7	8.5	3.6	0.3	38.8
SO_3	0.5	0.4	0.5	0.5	0	39.8	0
SrO	0	0	0	0	0	0.4	0
TiO_2	0.2	0.3	0.5	0.9	0	0	0.6
K_2O	0.6	0.3	0	0.1	0.2	0	0
Cr_2O_3	0.2	0.5	0.7	0.1	0	0	0
Co_3O_4	<0.4	0	0	0	0	0	0
NiO	<0.4	0.1	0	0	0	0	0.1
CuO	<0.4	0.0	0	0	0	0	0
V_2O_5	0	0	0	0.1	0	0	0
Cl	0.1	0.0	0	0	0	0	0
F	0	1.5*	1*	0	0	0	0
CeO_2	0	0	0	0	0	0.2	0
Sum	100.9	98.03	99.7	79.2	58.8	71.1	85.4
LOI (1000 °C, 1 h)	−4.45	−0.4	−0.41	19.17	41.46	29.31	12.76

*close to detection limit.

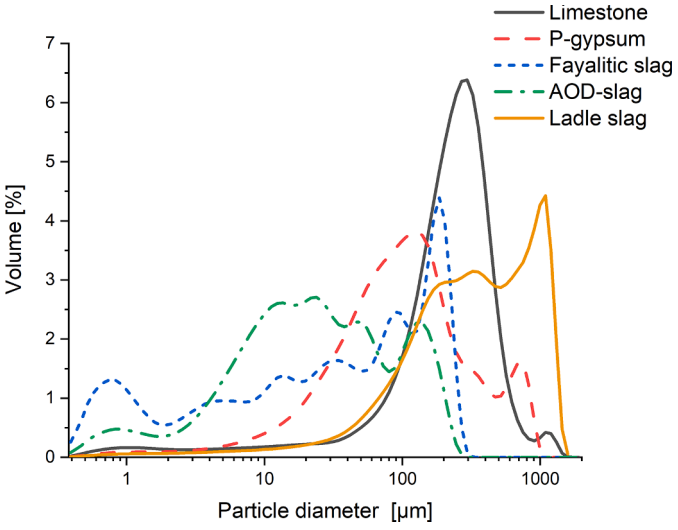

Fig. 1. Particle size distribution of the raw materials.

slag, phosphogypsum, and limestone were 22 μm, 36 μm, 334 μm, 99 μm, and 232 μm respectively. The procedure for PSD is explained in Section 2.1.3.

2.1. Methods

2.1.1. Pre-testing at laboratory scale

The fluorine content of the raw mix is an important factor for the formation of alite [9]. Too much fluorine is known to cause the melting of the clinker [9] and can lead to the blocking of the kiln during the semi-industrial trial. However, alite cannot form at 1260 °C and conventional residence times without enough mineraliser. The XRF analysis was found somewhat inaccurate when analysing the fluorine content of AOD slag. To identify much AOD slag could be used, a clinker was produced with an AOD slag content of 20 wt.%, with a target phase composition of 30 wt.% C_3S, 29 wt.% C_2S, 30 wt.% $C_4A_3\$$, 10 wt.% C_4AF, and 1 wt.% C$. The raw material mix for PRE LAB clinker was prepared according to the recipe shown in Table 3.

Table 3
Target phase composition, oxide content, and recipes for laboratory-scale pre-testing (PRE LAB (AOD 1)).

Target phases						
Phase	C_3S	C_2S	$C_4A_3\$$	C_4AF	CS (anhydrite)	
Wt.%	30	30	29	10	1	
Target oxide composition and required fluorine content						
Oxide	Al_2O_3	CaO	F*	Fe_2O_3	SiO_2	SO_3
Wt.%	16.6	57.3	0.37	3.3	18.4	4.4
PRE LAB (AOD 1)						
Raw material	Kaolin	AOD slag	$CaCO_3$	$CaSO_4$	Fayalitic slag	Ladle slag
Wt.%	9.4	20	45.5	10.4	3.8	42.9

*Target according to $X = 0.15$, $Ca_3Si_{1-x}Al_xO_{5-x}F_x$, which presents the fluorine substitution in the alite phase.

The calculations for the clinker recipes were made using the molar masses of the oxides to form the desired phases, similar to previous studies [9,15,31]. The amounts of industrial by-products needed to reach the oxide composition of each clinker recipes were adapted from the XRF analysis shown in Table 2. The previous studies on AYF clinkers have shown that the substitution of fluorine to alite has certain limitations. Too low content does not lead to alite formation and too high to formation of unwanted phases and decomposition of ye'elimite. The target for fluorine mineraliser content was adapted from [9], where it was found that with $X = 0.15$ in the formula of alite $Ca_3Si_{1-x}Al_xO_{5-x}F_x$, both alite and ye'elimite existed. X presents the substitution level of fluorine to alite in the empirical formula of pure alite phase. In accordance with cuspidine and CaF_2 content obtained from Rietveld analysis (appendix 3), it was assumed that the fluorine content of AOD slag (AOD 1) was around 2.8 wt.%. However, the fluorine content in XRF analysis was much lower and therefore it was assumed that fluorine content in fact is less.

The raw materials were weighed for 25 g of each clinker raw mix. The raw mix batches were then ground manually for ~20 min using a mortar and pestle to obtain a homogenous mixture. The batches were then put in crucibles and placed in an 800 °C pre-heated Nabertherm HT 08/18 chamber furnace 150 × 150 × 300 mm (Nabertherm GmbH, Germany), heated at a ramp rate of 7.6 °C/min (~1 h) to 1260 °C and held isothermally for 1 h. After the thermal treatment, the samples were

removed from the furnace at 1260 °C, and the materials were poured from the crucibles onto a copper table to quench in the ambient air. The copper table has inbuild water circulation to enhance the cooling speed. The cooled clinkers were ground by hand with an agate mortar and pestle into fine powders for XRD analysis.

2.1.2. Pilot kiln trial

The process parameters of the pilot kiln are shown in Table 4. A more detailed description of the kiln and pilot kiln trial can be found in [31], where the same equipment and procedure were used.

The 24 h time slot for the trial was divided into three different clinker recipes, PIL A, PIL B, and PIL C. The clinker raw mix recipes are presented in Table 5. The raw material mixes were weighed, mixed, and granulated to achieve a homogenous mix. Granulation was operated to decrease the material losses caused by the airflow. Granulation was done in 150 kg batches using a mixer equipped with star pin rotor (R11, Eirich, Germany). The granulation was operated as in [31] with exception that slightly higher amount of tap water (7–8 wt.%) was used. The total amounts each type of clinker produced were PIL A: 31 kg, PIL B: 20 kg, and PIL C: 27 kg. The transition materials between changing the clinker recipes were discharged. Clinker was discharged from the end of the kiln and cooled on a metal tray. It was estimated that the clinker will cool to ~1000 °C over a 10 min timescale. Cooled clinker was collected and packed in airtight plastic buckets.

2.1.3. Grinding, particle size distribution, and density of the clinkers

Prior to use, fayalitic the slag was ground in 30 kg batches using a stainless-steel jar mill (TPR-D, Germantec, Germany). The grinding was continued until all the material passed through a 100 μm sieve. The total average time for grinding each batch was around 4 h. The grinding media consisted of stainless-steel balls of d = 10 mm (20 kg), d = 25 mm (10 kg), and 50 mm (10 kg), and the jar diameter was $h = 0.6$ m and $d = 0.6$ m. The clinkers produced in the semi-industrial trial were separately ground using a ball mill with the same technique as for fayalitic slag, with the difference that the clinker was ground for 2–3 h until >85 % of the material passed through the 45 μm sieve. The quartering method was used for clinkers to collect representative samples for PSD, density, XRD, and XRF analyses to represent whole batches of semi-industrial clinkers PIL A: 31 kg, PIL B: 20 kg, and PIL C: 27 kg and to mix the clinkers. The PSD of the raw materials and the ground clinker was measured with a laser diffraction technique using the dry powder system module (LS 13 320, Beckman Coulter, USA) with the Fraunhofer model [32].

The density of the semi-industrial pilot clinkers with sample codes PIL A, PIL B, and PIL C was measured using a Gas Pycnometer (AccuPyc II 1340, Micromeritics, USA). The average density was calculated from a total of 20 analyses conducted for two samples from each clinker. The sample weights were between 6.5 and 8 gs. The standard deviations for the samples was between 0.0009 and 0.0018. The temperature of the testing was between 23.1 and 24.2 °C. Helium was used as a probe gas, the run pressure was set to 19.5 psig, and the pressure equilibration was 0.005 psig/min.

Table 4
Process parameters of the semi-industrial kiln trial.

Operation	Used in trial
Kiln length	7.4 m (7.0 m heated)
Kiln inner diameter	0.3 m
Refractory thickness	5 cm
Kiln inclination	1.0°
Kiln rotation speed	2 rpm
Heating method	Direct heating
Operating configuration	Counter current flow
Residence time	3 h
Raw meal feed (wet)	20 kg/h
Raw meal feed (dry)	~18.5 kg/h
Natural gas flow rate	20.1 ± 0.6 m^3/h
Oxygen flow rate (burner)	5 m^3/h
Oxygen volume kiln inlet	4.9 ± 0.7 Vol.-%
Clinkering zone temperature	1260 ± 6.5 °C
Exhaust cleaning	dust filter, cyclone

Table 5
Granule recipes for semi-industrial trial. Target phases were 30 wt.% alite, 30 wt.% belite, 30 wt.% ye'elimite, and 10 wt.% ferrite.

Recipe/clinker	PIL A		PIL B		PIL C	
Unit	kg	wt.%	kg	wt.%	kg	wt.%
Ladle slag	39.75	24.39	49.50	28.08	58.50	36.34
AOD slag (AOD 1)	18.00	11.04	24.00	13.61	28.50	17.70
Fayalitic slag	2.25	1.38	2.25	1.28	3.00	1.86
Phosphogypsum	11.25	6.90	11.25	6.38	12.00	7.45
Clay	18.00	11.04	13.50	7.66	9.00	5.59
Limestone	60.75	37.27	63.28	35.90	39.00	24.22
Added water	13.00	7.98	12.50	7.09	11.00	6.83
Weight of mix	163	100	176	100	161	100

2.1.4. XRF

The XRF analysis was conducted for raw materials, granules, and semi-industrial clinkers (PIL ABC). Loss on ignition (LOI) was measured from the raw materials presented in Table 2, which were collected using a 1.5 g sample size of each material separately placed in a pre-heated corundum crucible and heated to 1000 °C for 1 h.

Fayalitic slag was analysed using an Omnian Pananalytics Axiosmax 4 kV XRF spectrometer (Malvern Panalytical, UK). Pre-ground slag was further ground with a planetary mill at 300 rpm for 1 min. The melt fused bead from Fe slag was prepared using a fluxer (Eagon 2, Malvern Pananalytics, UK) by mixing 1.5 g of Fe slag in a platinum crucible with 7.5 g of X-ray flux Type 66:34 (66 % LiB_4O_7 and 34 % $LiBO_2$). The melting temperature of the fused beads was 1200 °C. The semi-industrial clinker and granules were analysed using the same method.

The rest of the raw materials shown in Table 2 were analysed using a Bruker S8 Tiger. The fused beads were prepared using a Spectromelt A12 (66 % $Li_2B_4O_7$/34 % $LiBO_2$) as flux. 1 g of the pre-heated sample material was mixed with 8 g of flux and melted in an automatic electric furnace (xrfuse2, XRF scientific, Australia) using Pt/Rh crucibles. XRF measurements were conducted with a wavelength dispersive X-ray spectrometer (S8 Tiger, Bruker, Germany) in vacuum conditions.

2.1.5. X-ray diffraction

The clinkers produced at laboratory scale were analysed using a Rigaku SmartLab 9 kW diffractometer in the Bragg-Brentano geometry equipped with a D/teX Ultra 250 detector. The XRD samples were ground using a mortar and pestle. The fine powder (<5 μm) was spread on a powder sample glass holder (20×20 mm with 300 μm well). Co Kα X-ray source (Kα1 = 1.78892, Kα2 = 1.79278) with a tube voltage of 40 kV and a tube current of 135 mA was used. XRD patterns were recorded with a step size of 0.02° in a range of 2-theta 5–130° and a scanning speed of 4.063 deg./min, totalling 6251 counts. The patterns were analysed using Rigaku PDXL 2 software with a PDF-4 + 2020 RDB database and Rietveld based Whole Powder Pattern Fit (WPPF) analysis. The Rietveld based WPPF analysis uses measured intensities together with crystalline structure, refinements to peak shapes, lattice parameters and preferred orientation. The Rietveld analysis for AOD slags was conducted using Pananalytical highscore software.

The phase composition of the semi-industrial clinkers was analysed using a Cu anode, 200 mm radius, automatic slits, a Soller slit of 2.5°, and no filters but an EDS (energy dispersive spectrometry) (D5000, Siemens, Germany; detector SolX, Bruker, USA). The diffractometer was operated with 40 kV and 40 mA. The patterns were recorded in the range of 2-theta 5–70° with a step size of 0.02°, totalling 3250 counts in the XRD pattern. The ground LAB B was analysed with an internal standard by mixing rutile (TiO_2) with the clinker to measure the amorphous content.

2.1.6. DTA-TG-MS

Differential thermal analysis (DTA), thermogravimetric analysis (TG), and mass spectrometry (MS) were conducted using paired STA449 (F3 Jupiter, Netzsch, Germany) and QMS403D (Aëolos Quadro, Netzsch, Germany). Before analysing, each granule sample was ground, and around 25 mg of the sample was placed on an alumina crucible. The heating ramp was set to 10 °C/min from room temperature to 1300 °C in an argon atmosphere with a gas flow of 60 ml/min. For mass spectrometry, the selected ions to be analysed were m/z = 17 (OH), 18 (H_2O), 28 (CO), 44 (CO_2), 48 (SO), 64 (SO_2), and 80 (SO_3).

2.1.7. Scanning electron microscopy combined with energy dispersive X-ray spectrometry (SEM-EDS)

Sample preparation. Ground clinker was collected from the batch, pressed into a tablet, and embedded in epoxy resin. Sample polishing was carried out using an automatic polishing device (TF250, JeanWirtz, Germany) and diamond oil pastes (MetaDi II, Buehler, US). Successive polishing with oil-based diamond pastes of 15, 9, 3, 1, and 0.25 μm was applied. To achieve electrical conductivity, the polished section was coated with approximately 8–10 nm carbon. The sample from AOD slag was prepared with the same method.

SEM imaging and eds spectroscopy. Back-scattered electron (BSE) imaging and EDS spectroscopy were used for microstructural characterisation (i.e. imaging, elemental mapping, and an analysis of the chemical composition of the major phases) of the produced clinker. BSE imaging and an EDS analysis were carried out at a 12 kV acceleration voltage and 0.8 nA electron current, using a high-resolution field emission SEM (Helios G4UX, ThermoScientific, USA) respectively. For the acquisition of EDS data, a silicon drift detector was used (X-Max80, Oxford Instruments, UK). This allowed elemental distribution maps to be collected at high resolution (approx. 0.1 μm pixel resolution) and high count number (~600 million counts per map). The EDS data acquisition and analysis were performed using commercial software (Aztec 4.3, Oxford Instruments, UK). The phase maps were deduced using the phase clustering algorithm implemented in the software (Aztec 4.3 and Aztec 5.0, Oxford Instruments). The quantification of the composition of the clinker phases was achieved by the calibration of the SEM-EDS setup against a pure cobalt standard. Iron content was determined using an Fe-L line. All other elements were quantified using the K-alpha lines of the respective elements.

2.1.8. The effect of the particle size of raw materials on phase formation (PIL b and ground pil B) and a comparison of the properties of aod 1 and aod 2 on phase formation (PRE lab (AOD 1) and (Post lab (AOD 2))

The particle size distribution of some of the raw materials was high for clinkering because the pre-treatment (grinding, sieving, etc.) for such quantities was impossible during the pilot trial. To ensure particle size did not affect the results of phase formation, a reference sample (Ground LAB B) from the granules (PIL B) presented in Table 5 was dried, ground to a fine powder (d_{50} = 6 μm) using a disc mill (Retsch, RS 200), and fired in a laboratory-scale muffle furnace. The clinker was then compared with the results of the XRD analysis of the pilot clinker, PIL B. POST LAB (AOD 2) was prepared in the same way as PRE LAB (AOD 1) clinker, described in Section 2.1.1, but with a different AOD slag.

2.1.9. Setting time of cement and mechanical testing

The produced clinkers were individually mixed with 12.5 wt.% anhydrite using a stainless-steel jar mill (10 L), with the grinding media consisting of 120 stainless-steel balls (d = 30 mm) for 20 min. The dry mixes were used to prepare samples for the mortars (compressive strength) and pastes (setting time). The W/B ratio for the mortars and pastes was 0.5, and EN 196–1 standard sand (Normesand, Germany) was used as aggregate. A citric acid–deionised water solution was used to retard the early hydration speed to improve workability. The solutions were PIL A (2 Vol-.%), PIL B (2 Vol-.%), and PIL C (0.5 Vol-.%). The citric acid content was reduced in the PIL C sample because the hydration was delayed too much with 2 Vol-.%. Reference PC (Portland cement, CEM II/B-M (S-LL) 42.5 N) cement was prepared without citric acid.

The setting times were measured from PIL A, PIL B, and PIL C using the Vicat apparatus (Matest E044 N, Italy) at 22 ± 1 °C according to the EN196–3 standard. The analysis was done using a cylindrical mould (inner d = 80 mm and h = 40 mm). The initial setting time was reported when the needle failed to pierce the sample beyond 6 ± 3 mm from the bottom, and the final setting time was reported when the distance from the needle to the bottom was 39.5 mm.

Compressive strength mortars were prepared from PIL A, PIL B, PIL C, and PC. A total of four batches was prepared to fill 40 mm x 40 mm x 160 mm prisms according to the EN 196–1:2005. standard. The batch size was 2025 g, including 450 g of clinker-anhydrite mix or PC, 1350 g of CEN standard sand, and 225 g of DI water–citric acid solution or DI water (PC). The cement was mixed using a laboratory-scale cement mixer (65-L0006/AM AUTOMIX), with the EN 196–1 programme selected. Mortar prisms were filled according to standard. After casting, the moulds with mortars were sealed in airtight plastic bags for 24 h to set. The prisms were then demoulded and submerged in water at a temperature of 20 °C. The compressive strength testing was conducted after 1, 3, 7, and 28 days of curing, using a Dartec 1992 (modernised in 2009 by Zwick/Roell) testing machine with a testing range of 0–400 kN. The testing machine was calibrated by Eurofins to reach the required accuracy for an accredited testing laboratory. The loading speed for the compressive strength test was 2400 N/s until fracture.

3. Results

3.1. Pre-tests at lab scale

The target phase composition for PRE LAB (AOD 1) clinker was 30 wt.% C_3S, 30 wt.% C_2S, 29 $C_4A_3\$$, 10 wt.% C_4AF, and 1 wt.% C$. The XRD analysis results for clinker produced in the pre-test is shown in Table 6, and the XRD pattern with phase identification is shown in Appendix 1, Figure A1. In pre-testing, it was found that 20 wt.% AOD slag provided enough fluorine for alite formation, alite could coexist with ye'elimite, and that AOD slag (AOD 1), fayalitic slag, and ladle slag could be used to achieve the desired cement phases. Phosphogypsum was unavailable for the pre-tests, and pure anhydrite was therefore used instead. The role of phosphogypsum was tested (see Appendix 2) with different target compositions, and it was found that alite could form with phosphogypsum.

The major phases of PRE LAB (AOD 1) clinker were C_3S, C_2S, $C_4A_3\$$, and C_2AF, and the minor phases were $C_{12}A_7$ and periclase (M). MgO from raw materials formed periclase (M), and mayenite was formed, which reduced the amount of ye'elimite. The pre-test results indicated that fluorite from AOD slag could be used to achieve the mineralising effect to form alite (C_3S).

3.1. Findings of the pilot kiln trial

3.1.1. DTA-TG-MS of pilot granules

Simultaneous differential thermal analysis (DTA),

Table 6
XRD Rietveld results of laboratory-scale pre-testing (PRE LAB (AOD 1)) with industrial by-products AOD slag, fayalitic slag, and ladle slag. Error of analysis and quality of the analysis R_{wp} were obtained from analysis software and was 3.1 %. Sum 100 %.

C_4A_3S	C_3S	C_2S	$C_2(A,F)$	$C_{12}A_7$	M	C_2AS	F-ell
[33]	[34]	[35]	[36]	[37]	[38]	[39]	[40]
12.1	24	28.8	13.7	6.2	5	3.6	6.7

thermogravimetric analysis (TG), and mass spectrometry (MS) were conducted for the granules to determine the gases emitted at certain temperatures during clinkering, and the results for the PIL B granules are shown in Fig. 2. The analysis results for PIL A and C (not shown here) were similar but with minor changes in water and carbon losses due to the differences between raw mixes.

Mass spectrometry peaks of m/z = 17(OH) were detected at three temperatures. Below 200 °C, the moisture evaporated, and gypsum decomposed to anhydrite at 170 °C [41]. $Al(OH)_3$ and kaolin decomposed at 300 °C [42] and 530 °C [43] respectively. Since water was added to the granules, other hydrates may also have been present, such as ettringite, C-S-H, etc. The peak of $m/z = 44(CO_2)$ at 800 °C shows the decomposition of limestone ($CaCO_3$). The highest peak of $m/z = 64(SO_2)$ was observed at 1233 °C, which was caused by the decomposition of anhydrite (phosphogypsum) [41]. The total mass loss of DTA-TG from room temperature up to 1300 °C was 32 wt.%, most of which was caused by the loss of H_2O and CO_2. The DTA curve shows that phase formation started after 900 °C.

3.1.2. Analysis of pilot granules and clinkers

The particle size distribution (PSD) of clinkers is presented in Fig. 3. The median particle sizes d_{50} for PIL A, PIL B, and PIL C were 5.5 μm, 5.6 μm, and 3.7 μm, respectively. D_{10} was around 0.7 μm for all the samples and d_{90} for PIL A, PIL B, and PIL C were 46.9 μm, 49.6 μm, and 22.9 μm, respectively. The procedure for grinding, mixing and PSD measurement is explained in Section 2.1.3. The measured average densities for the PIL A, PIL B, and PIL C samples were 3.1 g/cm^3, 3.2 g/cm^3 and 3.2 g/cm^3 respectively. The PSD of ground LAB PIL B clinker was measured separately, and the median particle (d_{50}) was 3.87 μm.

The phase content of the recorded XRD patterns shown in Fig. 4 for PIL A, PIL B, and PIL C was analysed with Rietveld analysis, and the results are shown in Table 7. The Rietveld analysis for Ground LAB B was added and is presented in Table 7 to compare the effect of the homogenisation of raw materials (grinding) on the phase formation. The major phases detected were larnite (β-C_2S), ye'elimite ($C_4A_3$$), ferrite C_2(A,F), mayenite ($C_{12}A_7$), and periclase (MgO). The minor phases were fluorite (CaF_2), ternesite ($C_5S_2$$), gehlenite (C_2AS), tricalcium aluminate (C_3A), an iron-rich solution of ferrite (C_2F), akermanite (C_2MS_2), anhydrite (C $), SiO_2 (S), perovskite (CT), and titanomagnetite (FeOT). Ground LAB B was analysed with an internal standard rutile (TiO_2) to prove that the amorphous content was close to 0.

It was found that no alite was present in any of the pilot clinkers, and the clinkers produced were BYF (belite–ye'elimite–ferrite) clinker with

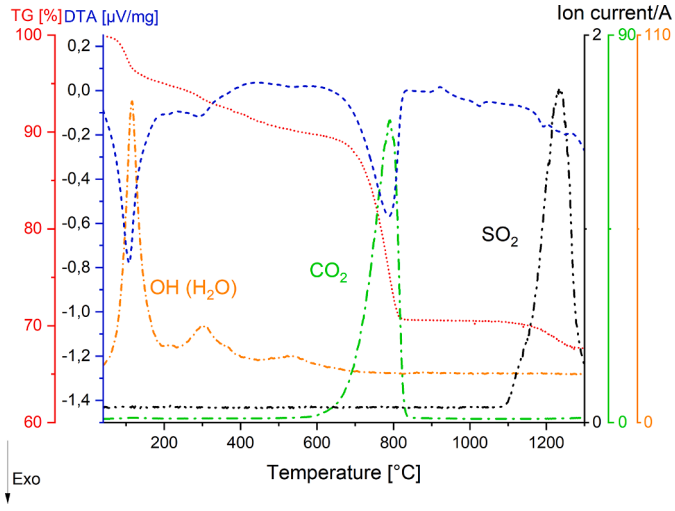

Fig. 2. DTA-TG-MS curves from raw meal granules of PIL B with a mass spectrometry analysis of H_2O, CO_2, and SO_2 gases. Argon atmosphere, 10 °C/min 30–1300 °C.

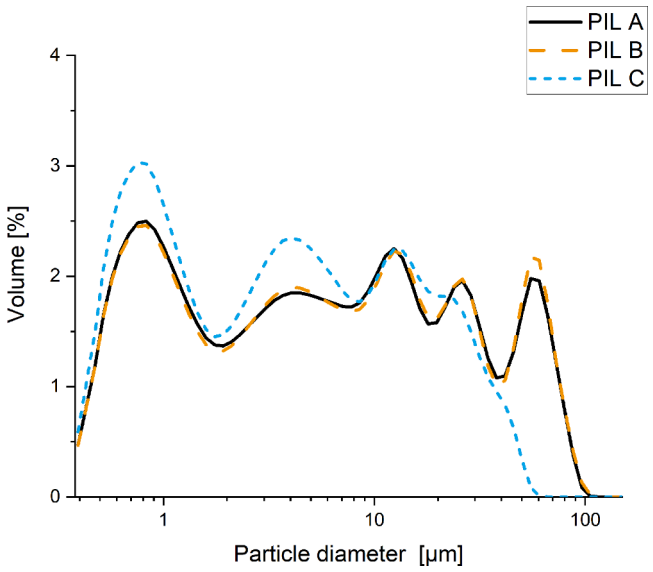

Fig. 3. Particle size distribution of ground clinkers PIL A, PIL B and PIL C.

significant quantities of mayenite and periclase instead of the targeted AYF clinker. The XRD analysis showed that the phase content of three produced clinkers was quite similar. The grinding of granules (Ground LAB B) and firing in laboratory conditions only slightly affected the phase composition. To confirm the findings of the XRD analysis, the results were compared with the target oxide composition and XRF analysis of the clinker. Table 8 shows the target oxide composition of the pilot clinkers, the XRF analysis of the granules, the XRF analysis of the clinker, and the calculated oxide composition, using the Rietveld phase abundances from Table 7. The target oxide compositions are presented with and without MgO to facilitate the comparison between the XRF results and the back-calculated compositions from XRD. The LOI content of granules at 950 °C was PIL A: 24 wt.%; PIL B: 21.6 wt.%, and PIL C: 18 wt.%.

More than 90 wt.% of the oxides in the XRF analysis of the clinker and granules consisted of the target oxides needed to form hydraulic cement phases. The XRF analyses showed that the oxide compositions of granules were mostly in agreement with the target composition (calculated with MgO), but the raw material mix of the granules was diluted with impurities. The difference between the calculated target and the XRF analysis of the granules was as follows: less lime in PIL B and PIL C, less alumina in all clinkers, and more iron in all clinkers.

MgO was the largest impurity in the clinkers according to the XRF analysis. The limit for MgO content in dry cement (PC) is between 5 and 6 wt.%, depending on local standardisation [53]. The MgO content in the produced clinkers was between 5.1 and 6.0 wt.%, but the MgO content was diluted when the clinker was mixed with gypsum to make the cement dry mix, and the MgO content therefore did not restrict the use. Fluorine could not be detected in the clinkers, and it was only detected in the granules of the PIL C mix. However, fluorine could be detected in the EDS analysis of AOD slag, the XRD analysis of all clinkers as CaF_2, and was also found in the XRF analysis of the kiln inlet material/tailing (Appendix, Table A2). This indicates that there was fluorine in both the granules and the clinker, but the content was below the detection limit of XRF. The differences between the oxide content of granules (XRF) and clinker (XRF) and back-calculated oxide composition from Rietveld phase (XRD) abundances are compared in Table 9.

The results in Table 9 show that the iron content increased in all the clinkers, and the lime and sulfur content decreased during burning. An increase in the iron content between granules and clinker was present in all the clinkers PIL A (57 %), PIL B (42.5 %), and PIL C (53 %). There was a high gas velocity in the kiln from the burner, which may have carried

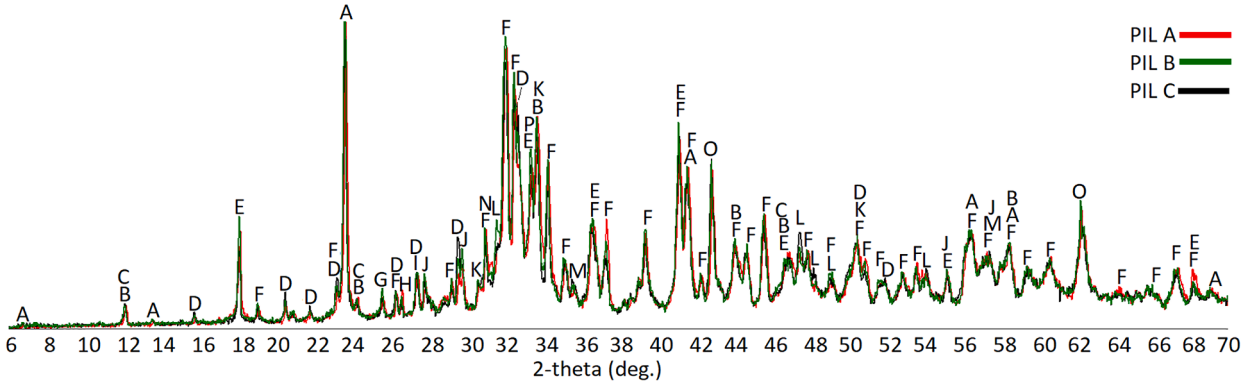

Fig. 4. XRD pattern of PIL A (red line), PIL B (green line), and PIL C (black line) pilot clinkers with phase identification. A: $C_4A_3\$$, B: $C_2(A,F)$, C: C_2F, D: γ-C_2S, E: $C_{12}A_7$, F: β-C_2S, G: C$, H: SiO_2, I: C_2AS, J: C_3A, K: $C_5S_2\$$, L: CaF_2, M: FT, N: C_2MS_2, O: MgO and P: CT.

Table 7
XRD analysis of reference clinkers produced in laboratory furnace and pilot clinkers after firing, grinding, and mixing. The error of analysis and the quality of the analysis R_{wp} were obtained from the analysis software. Ground LAB B was analysed with an internal standard rutile (TiO_2), and the amorphous content was close to 0.

Phase	Reference	Target phases [wt.%]	Pil A [wt. %]	Pil B [wt. %]	Pil C [wt. %]	Ground LAB B [wt. %]
β-C_2S	[44]	30	42.8	41.3	39.5	49.1
$C_4A_3\$$ (orto)	[45]	29	17.2	16.7	16.6	13.9
$C_2(A,F)$	[36]	10	6.9	6.7	7.2	9.4
C_3S	[34]	30	0.0	0.0	0.0	0.0
γ-C_2S	[44]	0	4.2	6.4	10.3	3.7
$C_{12}A_7$	[37]	0	8.0	7.5	6.5	7.9
M	[38]	0	4.5	4.6	5.6	5.3
CaF_2	[46]	0	0.8	0.9	0.9	1.5
$C_5S_2\$$	[47]	0	3.6	4.2	3.3	2.9
C_2AS	[39]	0	1.3	1.6	0.8	0.8
C_3A	[48]	0	1.8	2.4	2.2	0.7
C_2F	[36]	0	1.4	0.8	1.0	0.1
C_2MS_2	[39]	0	3.2	2.4	2.0	0.7
C$	[49]	1	0.8	1.3	1.0	1.3
S	[50]	0	0.5	0.2	0.2	0.0
CT	[51]	0	2.0	2.0	1.9	2.2
FeOT	[52]	0	0.9	1.0	1.0	0.6
C		0	0.0	0.0	0.0	0.0
R_{wp} [%]			9.98	9.78	9.02	9.05

*High R_{wp} is due to rutile addition to the sample and the high background of a detector.

light raw materials (gypsum, limestone, etc.) to the front of the kiln where it was collected as kiln inlet material/tailings. This may partly explain the higher iron and lower lime and sulfur content in the final clinker than in the granules. Furthermore, Section 3.1.1 shows that some of the sulfur was lost at elevated temperatures as gas. The loss of sulfur during firing was also observed as an average of 60 ppm (SO_2) in near-infrared analysis (NIR), which was measured from the kiln inlet. The high TiO_2 content in the back-calculation of Rietveld analysis shows that perovskite and titanomagnetite content may be overestimated in the XRD analysis. The SiO_2-containing phases were also slightly over-estimated. The AC content was found to be close to 0, and does not explain the difference.

The SEM-EDS analysis was performed for the clinkers PIL A, PIL B, PIL C, and PIL B LAB to identify phases and their chemical composition. The major and minor phases of clinker PIL B are identified in Fig. 5.

The major phases found by SEM-EDS agree with the phases found by the XRD analysis. In addition to the target major phases, there are eight minor phases, four of which are supposedly phases originating from the raw materials. The clinker phases formed clusters of phases in tens of micrometres, with the size of individual phases below a diameter of 5–10 μm. The unreacted raw materials have a significantly larger particle size (CA, CSMA/CSAM (Ca-Mg-Al-silicate), CaO, etc.).

Contrary to what was expected, alite (C_3S) could not be detected by EDS and XRD analysis. Hence, fluorine was designed to act as a mineraliser. Its fate in the clinker was analysed more precisely. Fluorine was tracked in all the pilot trial clinkers. As already detected by XRD, fluorine was present as CaF_2 and is shown in samples PIL A (Appendix, Figure A4), PIL B (Appendix, Figure A5), and PIL C (Fig. 6). The results in Table 10 and Fig. 6 show that besides CaF_2, fluorine was substituted by ternesite ($C_5S_2\$$), mayenite $C_{12}A_7$), and a calcium silicate phase, with 14 % of fluorine (Fig. 6).

The chemical phase compositions for the phases identified in Fig. 5 are shown in Table 10. It can be seen that four different forms of ferrite with different Fe, Al, and Ti content are differentiated by PA. The results are shown in at-.% to allow a comparison between F and other elements.

To confirm that particle size did not cause the variation in the results, a reference sample (Ground LAB B) from the granules (PIL B) was also analysed with EDS. The phase map and elemental distribution maps of the impurities are presented in Fig. 7, and the average chemical composition of each phase can be found in Appendix 1, Table A3.

The grinding of granules (Ground LAB B) before firing in laboratory conditions made the distribution of the clinker phase more homogenous, and it seems that fewer relics from the raw materials were observed. The major phase composition (C_2S, $C_4A_3\$$, and $C_2(A,F)$) of the clinker remained the same as in the clinker produced in the pilot kiln. Again, alite (C_3S) was not observed. The minor phases here were also mayenite $C_{12}A_7$, periclase (MgO), ternesite ($C_5S_2\$$), and fluorite (CaF_2). The minor elements Ti and Mn were bound to the ferrite phase. Elemental distribution mapping showed that the fluorine had concentrated to CaF_2, which even in laboratory conditions, did not react, with grinding and optimal heat treatment at 1260 °C.

3.1.3. Comparison of pre-test and pilot AOD slags (Post LAB (AOD 2))

As it was found in the pre-tests that alite was formed, but that there was no alite formation in the pilot clinkers, clinker was prepared in laboratory conditions using the same AOD slag (AOD 2) as in the pilot. The recipe for the clinker is presented in Table 3. The XRD analysis of the "post LAB (AOD 2)" clinker is shown in Table 11, and the XRD pattern with phase identification is shown in Appendix 1, Figure A2.

It was found that no alite was observed in the AOD slag used for the pilot. This indicates that the AOD slag used in the pilot may have had different fluorine content or another issue that prevented its utilisation as a mineraliser and thereby the formation of alite.

Table 8
Target oxide composition of clinker with and without MgO in target. XRF analysis of granules and clinker (PIL A, B, and C). The original elemental wt.% obtained from the analyses is converted to oxides and normalised. The LOI of granules was PIL A: 24 wt.%; PIL B: 21.6 wt.%, and PIL C: 18 wt.% at 950 °C, and the LOI of the clinkers was negligible. The XRF values are compared with the recalculated oxide composition from the Rietveld phase abundances shown in Table 7.

	Target		PIL A			PIL B				PIL C		
Analysis/ oxide	Target	Target MgO	XRF granules	XRF clinker	XRD clinker	XRF granules	XRF clinker	PIL B (XRD)	Ground LAB B (XRD)	XRF granules	XRF clinker	XRD clinker
CaO	56.9	53.7	53.6	51.3	50.9	52.8	49.5	51.2	51.8	50.5	50	50.8
Al_2O_3	16.5	15.6	14.1	15.1	15.3	13.5	14.7	15.0	13.4	14.3	14.6	14.1
SiO_2	18.2	17.2	17.5	17.3	19.5	17.4	17.4	19.3	19.8	17.8	17.5	19.3
Fe_2O_3	3.3	3.1	3.5	5.5	3.8	4.7	7.2	3.4	3.5	4	5.7	4.2
SO_3	4.4	4.1	4.3	3.7	3.3	4.4	3.7	3.6	3.1	5	3.8	3.3
MgO	0	5.6*	5.1	5.1	5.0	5.4	5.3	5.0	5.4	5.9	6	5.8
BaO						<0.1				<0.1		
CaF_2	0.76	0.7	0	0	0.8	0	0	0.9	1.4	0.82	0	0.9
Cl			0	0		0	0.1			0.1	0.1	
Co_3O_4			0	<0.1		0	<0.1			<0.1	0	
Cr_2O_3			0.2	0.2		0.2	0.2			0.2	0.3	
CuO			<0.1	<0.1		<0.1	<0.1			<0.1	<0.1	
K_2O			0.2	0.2		0.2	0.1			0.1	0.1	
MnO			0.3	0.5		0.4	0.5			0.5	0.6	
Na_2O			0.2	0.1		0.1	0.1			0.1	0.1	
Nb_2O_5			<0.1	<0.1		<0.1	<0.1			<0.1	<0.1	
NiO			<0.1	0.1		<0.1	0			<0.1	0.1	
P_2O_5			0.1	0.1		0.1	0.1			0.1	0.1	
SrO			0.1	0.1		0.1	0.1			0.1	0.1	
TiO_2	0	0	0.7	0.7	1.5	0.7	0.7	1.6	1.5	0.7	0.7	1.5
V_2O_5			0	0.1		0	0.1			0	0.2	
ZnO			<0.1	0		0	<0.1			0	0	
ZrO_2			<0.1	<0.1		<0.1	<0.1			<0.1	<0.1	
Total	100	100	100	100	100	100	100	100	100	100	100	100
R_{wp}					9.98			9.78	9.02			9.02
F	0.5	0.4	0	0	0.4	0	0	0.4	0.7	0.4	0	0.5

*Estimated MgO from raw materials.

Table 9
Difference of the normalised oxide contents of the granules and clinkers (XRF analysis) and the difference between the oxide content of clinkers deduced by XRF and oxide content recalculated from XRD Rietveld analysis.

XRF granules – XRF clinkers	Deviation of oxide [wt%]	Change of oxide [wt%]	Change of oxide [wt%]
Oxide	**PIL A**	**PIL B**	**PIL C**
CaO	2	3	0
Al_2O_3	−1	−1	0
SiO_2	0	0	0
Fe_2O_3	−2	−3	−2
SO_3	1	1	1
MgO	0	0	0
CaF_2	0	0	1
Comparison of XRF clinkers – Rietveld	**Change of oxide [wt%]**	**Change of oxide [wt%]**	**Change of oxide [wt%]**
Oxide	**PIL A**	**PIL B**	**PIL C**
CaO	0	−2	−1
Al_2O_3	0	0	1
SiO_2	−2	−2	−2
Fe_2O_3	2	4	2
SO_3	0	0	1
MgO	0	0	0
TiO_2	−1	−1	−1
CaF_2	−1	−1	−1

3.1.4. Setting time and mechanical testing of pilot clinkers

The setting time of the three pilots and reference commercial PC cement pastes were tested, and the results are shown in Table 12.

The setting time is increased with more AOD slag in the raw mix. This can be explained by the increased content of poorly hydrating γ-C_2S [54] shown in the XRD analysis. Mayenite and ye'elimite content in clinkers can lead to flash setting as seen by [55], and citric acid has been seen to effectively prevent flash setting and increase the workability of pastes [56]. Fluoride is known to affect hydration speed. In CSA mixes, it is reported to have a retarding effect [57,58]. In PC, a small amount of fluoride works as an accelerator, but the effect changes to retarding after a certain threshold [6,59]. Despite the reduced hydration, the final strength is reported to reach the same or a higher level as fluoride-free cement [6,60].

The compressive strength data (Fig. 8) show that the best performance from the prepared pilot clinkers was achieved with PIL A and PIL B. PIL C showed slow strength development. The 28-day performance of the clinkers was roughly between 30 and 35 MPa. None of the prepared clinkers reached the 28-day performance of the reference PC cement (CEM II/B-M (S-LL) 42.5 N).

4. Discussion

The existence of the fluorine-bearing phases CaF_2 and cuspidine in AOD slag 2 could be proven by the XRD and EDS analyses, but the absolute fluorine content of AOD slag was difficult to determine with XRF analysis because of detection limitations. It is known that too much fluoride in the ye'elimite-alite system reduces ye'elimite content and leads to the formation of mayenite and the melting of the clinker [9]. The melting may have led to the blocking of the kiln during the semi-industrial trial. Hence, the safe limit for using AOD slag is to adjust the fluorine content in the raw mix. The pre-tests showed that 20 wt.% AOD slag in the raw mix was enough to provide fluoride for a mineralising effect to form alite at 1260 °C. The raw mix was prepared from 48.1 wt.% of ladle slag, 20 wt.% of AOD slag, and 4.2 wt.% of fayalitic slag. The reagent-grade chemicals were prepared to adjust the composition for the production of the target phase composition of 30 wt.% C_3S, 30 wt.% C_2S, 29 wt.% $C_4A_3\$$, 10 C_4AF, and 1 C$. The XRD analysis of the pre-test clinker (PRE LAB (AOD 1)) verified the formation of alite.

The AOD slag in the semi-industrial trial was obtained from a different production batch than in pre-tests, but according to XRF, the chemical composition (Table 2) and XRD patterns (Appendix 1, Figure A7) were very similar. After the experiments it was found from Rietveld analysis (Appendix 3, Figure A10 and A11) that the cuspidine

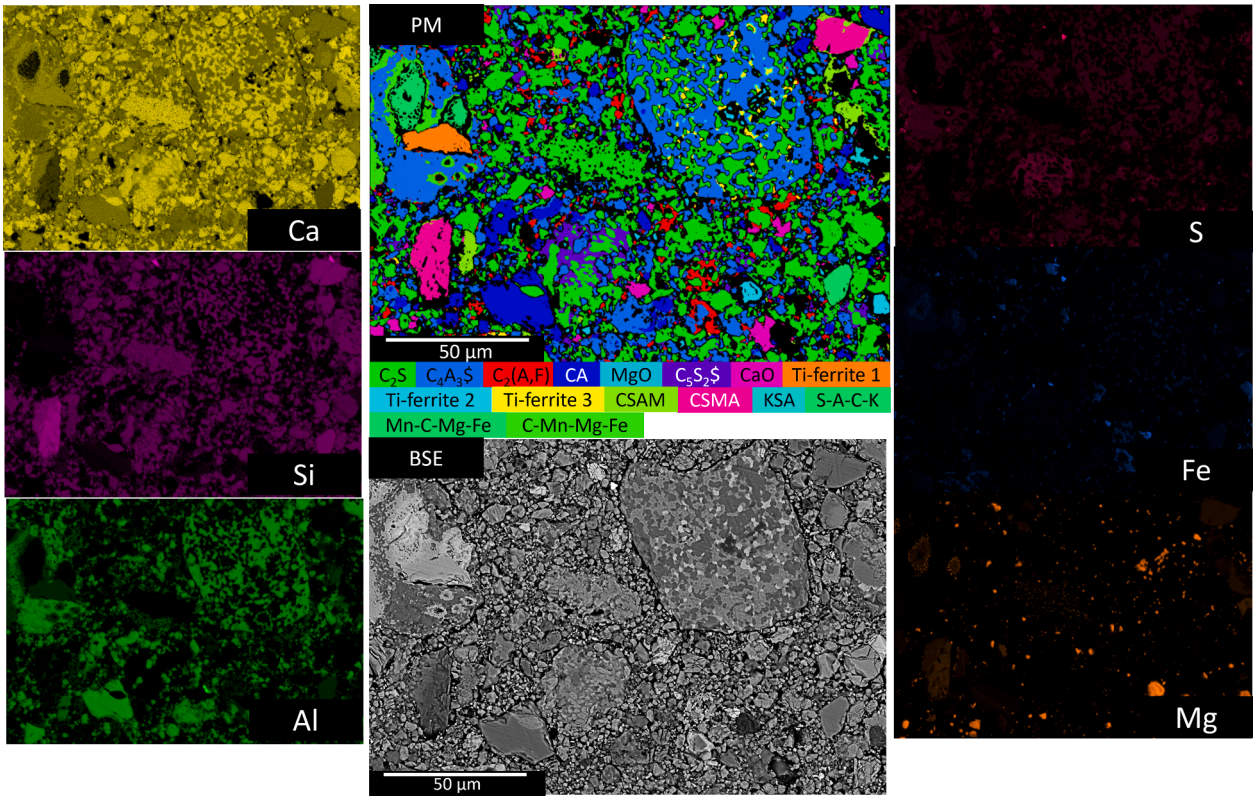

Fig. 5. Results of the EDS mapping analysis of PIL B clinker: elemental distribution maps were used to calculate the phase map (PM). PM shows the major phases of belite (C_2S), ye'elimite ($C_4A_3\$$), four different types of ferrite $C_2(A,F)$, mayenite (CA; $C_{12}A_7$), and periclase (MgO). The minor phases were ternesite ($C_5S_2\$$), free lime (CaO), CSAM-CSMA, and were associated with the gehlenite (C_2AS) – akermanite (C_2MS_2) series. KSA, S-A-C-K, Mn-C-Mg-Fe, and C-Mn-Mg-Fe are probably residues from the raw material. Elemental distribution maps for minor elements are presented in the Appendix in Figure A6.

content in AOD slag 2 was significantly lower when compared to AOD slag 1. In the semi-industrial trial, the AOD slag content in the raw mix was 12 wt.%, 16 wt.%, and 19 wt.% for PIL A, PIL B, and PIL C respectively. When the LOI (27 wt.%) was compensated for on the dry basis, the amount of AOD slag in raw mixes was 15.2 wt.% for PIL A, 20.3 wt.% for PIL B, and 24 wt.% for PIL C. During the pilot test, no melting occurred in any raw mix, and alite did not form. According to the XRD analyses, the only difference in mineralogy with an increase of AOD slag in raw materials in PIL B and PIL C was an increased γ-C_2S and periclase (MgO) content. The increased γ-C_2S content in PIL B and PIL C led to a finer particle size distribution of the ground clinker because the volume of γ-C_2S was higher than β-C_2S [25]. The effect on hydration was also found to be negative, as γ-C_2S has poor hydraulic properties [54]. It was found that the increased presence of γ-C_2S led to a slow setting time and poor mechanical strength. It is also known that fluoride affects hydration times. After the pilot demonstration, the granules of PIL B were ground and refired in a muffle furnace. It was found that the relatively large particle size of the raw materials in the semi-industrial trial only had a minor effect on phase formation, but fewer relics from the raw materials were present when the granules were ground prior to firing.

After the semi-industrial pilot, it was found that the AOD slag used in the semi-industrial trial had different properties than the clinker used in the pre-tests. The pre-test clinker was repeated with both AOD slags, and it was found that using the AOD slag used in the semi-industrial trial did not lead to the formation of alite. Sulfur can incorporate belite and alite as S^{6+} to replace Si^{4+}, but it heavily favours belite, so sulfur in the raw mix leads to the formation of belite and free lime instead of alite at low production temperatures [54,61]. The presence of sulfur does not explain the absence of alite because alite could have been formed in the laboratory-scale testing from the first batch of AOD slag. According to the XRD analysis, minor amounts (3–4 wt.%) of ternesite ($C_5S_2\$$) were present in the produced clinkers. Phosphates and fluorides can be used as mineralisers to enhance the formation of ternesite at temperatures higher than 1200 °C [62]. It is reported that CaF_2, P_2O_5, and Na_2O in the raw mix can enhance the coexistence of ternesite and ye'elimite. Na_2O and CaF_2 had the strongest mineralisation effect on ternesite [63,64]. The EDS analysis showed that PIL B had ternesite with 2.6 at.-% (Table 10) and pilot B lab clinker 4.5 at.-% (Table A3) fluorine substitution, and 0.1–0.2 at.-% Na was detected. This suggests that impurities from raw materials had a strong influence on ternesite formation. The results show that if AOD slag is designed to be used as a raw material and as a CaF_2 source for AYF clinker manufacture, the fluorine content of the slag needs to be very carefully analysed. This could be achieved by mixing a big batch of AOD slag in which the F content is precisely analysed, allowing the optimisation of the AOD content in the raw mix.

5. Conclusions

At the laboratory scale, AOD slag 1 (Table 2) with other industrial by-products was utilised to produce AYF (alite-ye'elimite-ferrite) clinker. Fluorine-bearing industrial by-product AOD slag could be used as a fluorine source to replace CaF_2 to produce a clinker in the laboratory furnace at 1260 °C, where both a ye'elimite and alite phase were present. According to the laboratory tests (PRE LAB), the produced clinker also had belite with alite and ye'elimite because sulfur effectively stabilised it. At the semi-industrial pilot scale, AOD slag 2 with ladle slag, fayalitic slag, and phosphogypsum was utilised to produce AYF clinker in a 7 m directly heated rotary kiln because the fluorine content of the slag was hard to determine accurately. The clinkers were produced with three different quantities of AOD slag in order to have an increasing fluorine content in the raw mix. The final clinker was found to be BYF

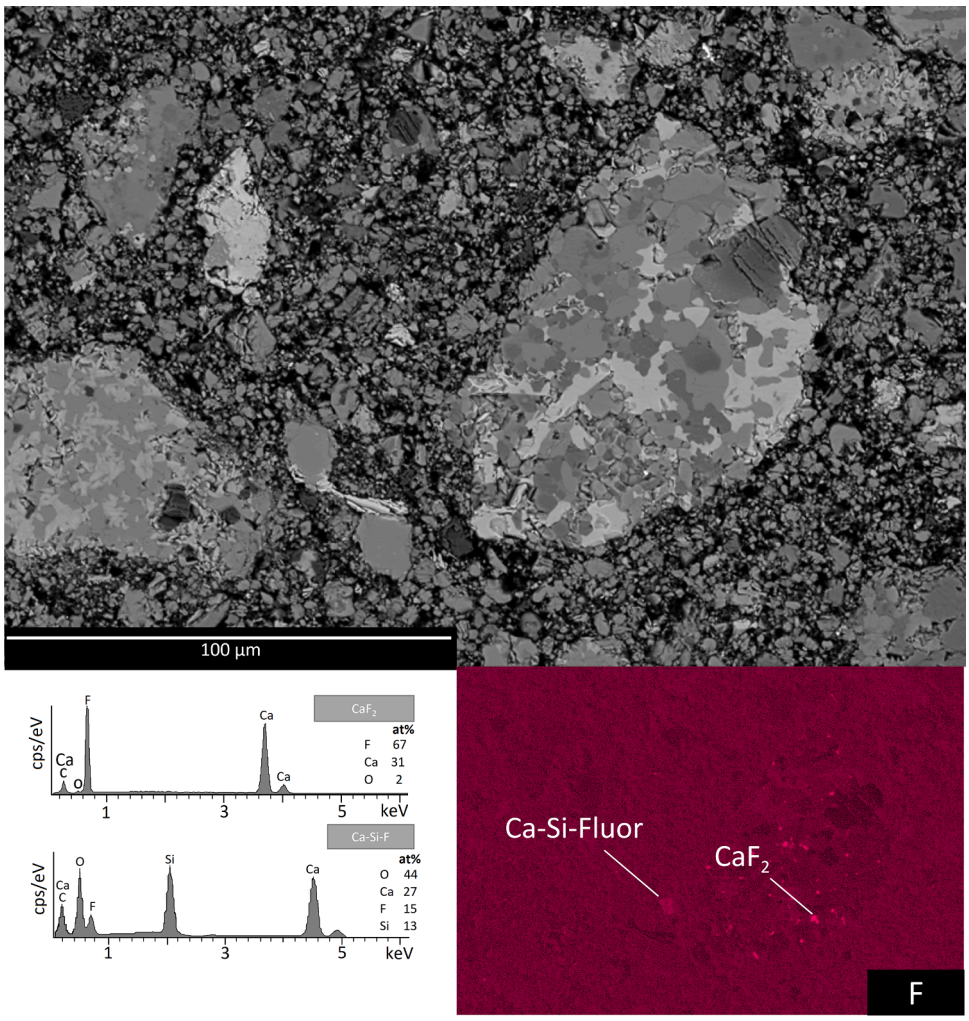

Fig. 6. Results of the EDS mapping analysis of Pil 2C: (Ca) and fluorine (F) are shown. The fluorine-bearing calcium silicate (cuspidine) and fluorite (CaF_2) are marked in the figure, and the chemical analyses from the single analysis points of Ca-Si-F phase and CaF_2 are shown in the bottom left-hand corner.

Table 10
Average chemical composition (given in at-%) of the clinker phases of PIL B in EDS analyses.

Phase/oxide	O	Ca	Si	Al	Mg	S	Fe	Na	Ti	Mn	F	K	Sum
Belite	57.4	26.6	13.3	1.4	0.5	0.4	0.2	0.1	0.0	0.0	0.0	0.0	100
Ye'elimite	59.1	15.6	1.7	19.1	0.3	3.3	0.6	0.1	0.0	0.2	0.0	0.0	100
Ferrite	56.6	20.7	2.4	9.9	1.2	0.9	6.1	0.0	1.1	1.0	0.0	0.0	100
Mayenite	55.7	17.8	1.2	21.8	0.8	0.3	0.5	0.1	0.0	0.0	1.6	0.0	100
Ternesite	58.5	23.2	8.4	1.3	0.2	5.3	0.0	0.2	0.2	0.0	2.6	0.0	100
Ti-ferrite 1	58.3	19.9	1.2	8.1	0.5	0.0	1.0	0.0	8.3	0.9	0.0	0.0	99
Ti-ferrite 2	58.0	18.3	2.6	11.0	0.6	1.3	4.1	0.0	3.1	0.9	0.0	0.0	100
Ti-ferrite 3	57.3	20.0	3.0	5.2	1.2	0.3	6.8	0.0	4.7	1.2	0.0	0.0	100
CSAM	58.3	17.3	13.1	5.7	4.3	0.2	0.6	0.3	0.0	0.1	0.0	0.0	100
CSMA	59.3	12.3	18.2	1.0	7.9	0.0	0.5	0.4	0.0	0.0	0.0	0.3	100
KSA	56.5	2.4	12.7	11.8	0.6	0.0	1.6	1.2	0.5	0.0	0.0	12.8	100
S-A-C-K	60.1	11.2	16.0	6.5	0.3	0.0	2.6	0.8	0.4	0.0	0.0	1.7	100
Mn-C-Mg-Fe	52.0	10.9	0.2	1.2	9.8	0.0	6.6	0.0	0.0	19.4	0.0	0.0	100
C-Mn-Mg-Fe	55.0	20.5	0.8	10.7	1.3	0.7	3.5	0.0	0.7	6.4	0.0	0.0	100

(belite-ye'elimite-ferrite) clinker instead of AYF. The ye'elimite had minor substitutions with iron, belite was present in both γ- and β-C_2S polymorphs, and the ferrite phase was present with various quantities of titanium, iron, and alumina. The content of γ-C_2S increased with more AOD slag in the raw mix. The most notable minor phases were mayenite, periclase, gehlenite-åkermanite, ternesite, and fluorite. Ternesite was found to have a substitution of fluorine and sodium, which were found to be common elements for stabilising ternesite in a system in which ye'elimite was also present. At the laboratory scale, AOD slag 1 was found to be suitable raw material for producing alite-ye'elimite clinker, but AOD slag 2 could not be utilized even under laboratory conditions. This may be because the fluorine content in AOD slag 2 was too low, or because an unknown factor prevented the decomposition of the fluorine-bearing minerals in the AOD slag during firing, but this could not be

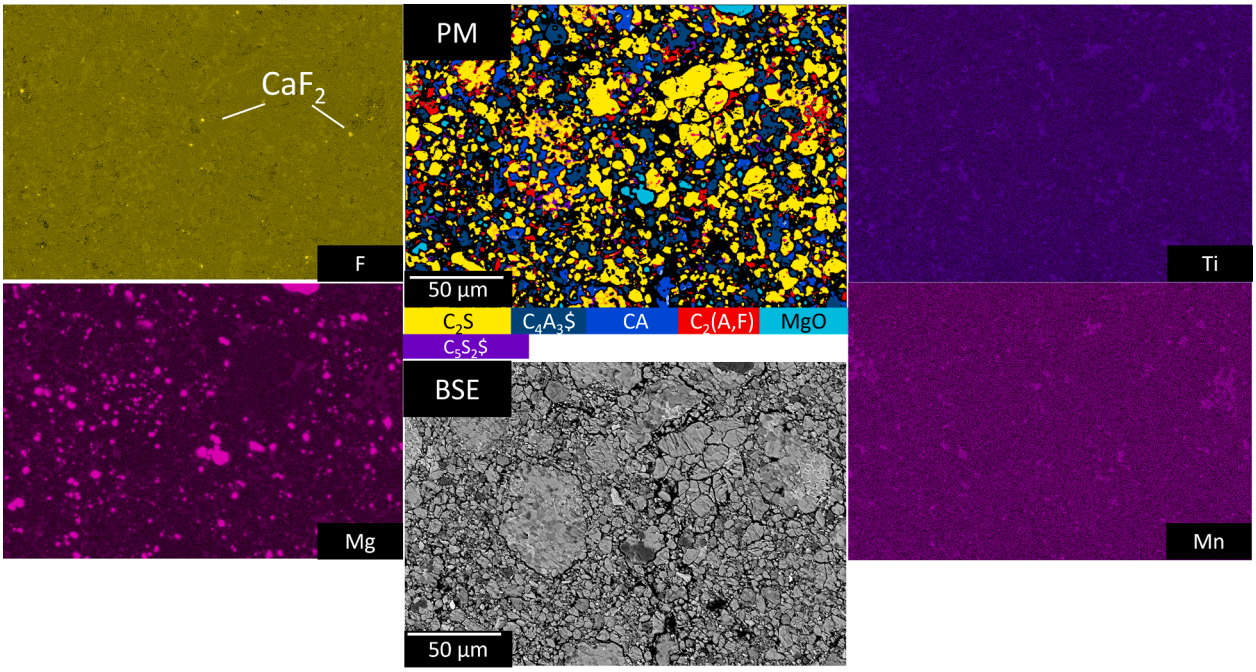

Fig. 7. Results of the EDS mapping analysis of ground LAB B clinker: the phase map (PM) differentiates the following phases: belite (C_2S); ye'elimite ($C_4A_3\$$); ferrite $C_2(A,F)$; mayenite (CA; $C_{12}A_7$); periclase (MgO); and ternesite ($C_5S_2\$$). Because of its small size, CaF_2 is identified only in the elemental distribution map of fluorine (F) as light dots.

Table 11
XRD Rietveld results for PIL B clinker prepared at laboratory scale from AOD slag used for the pilot (POST LAB (AOD 2)). Error of analysis and quality of the analysis R_{wp} were obtained from analysis software and was 3.5 %.

$C_4A_3\$$	C_3S	C_2S	$C_2(A,F)$	$C_{12}A_7$	M	C_2AS	F-ell
[33]	[34]	[35]	[36]	[37]	[38]	[39]	[40]
7.3	0	39	12.6	17.2	6.5	8.8	8.6

Table 12
Setting time of PIL A, PIL B, PIL C, and reference PC cement pastes tested with Vicat apparatus.

	PIL A	PIL B	PIL C	PC
Initial [min]	47	54	158	242
Final [min]	87	167	685	385

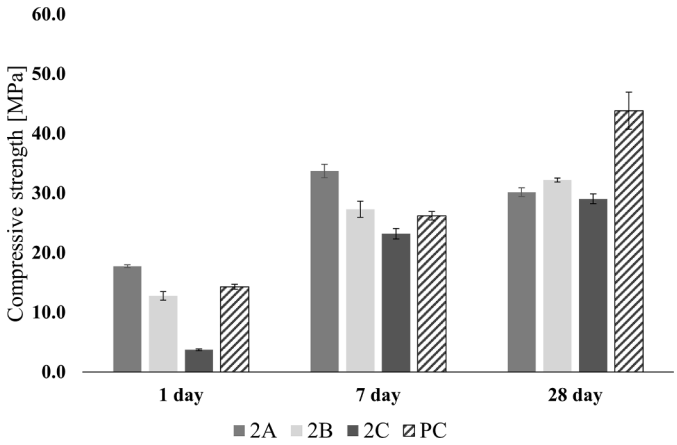

Fig. 8. The compressive strength of PIL A, B, and C compared with commercial PC cement 1, 3, 7 and 28days after the curing.

proven in this study. It was found from XRD Rietveld analysis that cuspidine content of AOD slag 2 was lower than in AOD slag 1. However, the absolute fluorine content in the slags could not be determined in this study. A better chemical and mineralogical characterisation of AOD 2 slag is required to determine why it did not have a mineralisation effect in producing alite. The results suggest that the production of AYF clinker at the pilot scale may be possible with AOD slag 1, which was found to be successful at the laboratory scale.

CRediT authorship contribution statement

Visa Isteri: Conceptualization, Methodology, Validation, Formal analysis, Investigation, Visualization. **Katja Ohenoja:** Conceptualization. **Christiane Rößler:** Writing – review & editing, Writing – original draft, Validation, Software, Methodology, Investigation, Formal analysis, Data curation. **Holger Kletti:** Writing – review & editing, Writing – original draft, Software, Resources, Investigation, Formal analysis, Data curation. **Pekka Tanskanen:** Writing – review & editing, Writing – original draft, Supervision, Resources, Project administration, Investigation, Conceptualization. **Mirja Illikainen:** Writing – review & editing, Supervision, Resources, Project administration, Funding acquisition, Conceptualization. **Theodore Hanein:** Writing – review & editing, Writing – original draft, Validation, Supervision, Methodology, Investigation, Formal analysis, Data curation, Conceptualization. **Timo Fabritius:** Writing – review & editing, Supervision, Resources, Project administration, Funding acquisition, Conceptualization.

Declaration of competing interest

The authors declare that they have no known competing financial interests or personal relationships that could have appeared to influence the work reported in this paper.

Data availability

Data will be made available on request.

Acknowledgements

This study was undertaken as part of the CECIRE project (1415/31/2015), supported by Business Finland and the following companies: Boliden Harjavalta; Boliden Kokkola; Yara Suomi; Fortum Waste Solutions; and Outokumpu Stainless. T. Hanein's participation was funded by UKRI FLF (MR/V023829/1) and EPSRC (EP/W018810/1). The authors would like to acknowledge IBUtec and Dr Martin Radke for setting up the pilot configuration and for technical support during the pilot study. The XRD, XRF, and FESEM analyses were performed at the Centre of Microscopy and Nanotechnology (University of Oulu) and the F.A. Finger Institute for Building Materials Science (Bauhaus University). We thank Simo Isokääntä from SSAB Europe Oy for providing ladle slag for the pilot kiln trial. We also thank the Tauno Tönning Research Foundation and the Walter Ahlström Foundation for their financial support for the study. Special thanks to the laboratory engineers of the process metallurgy laboratory, Tommi Kokkonen and Riku Mattila, and Jarno Karvonen, Elisa Wirkkala, and Jani Österlund from Fibre and Particle Engineering.

Supplementary materials

Supplementary material associated with this article can be found, in the online version, at doi:10.1016/j.cement.2024.100098.

References

[1] V.P. Masson-Delmotte, A. Zhai, S.L. Pirani, C. Connors, S. Péan, N. Berger, Y. Caud, L. Chen, M.I. Goldfarb, M. Gomis, K. Huang, E. Leitzell, J.B.R. Lonnoy, T. K. Matthews, T. Maycock, O. Waterfield, R. Yelekçi, Y. Zhou, B. Zhou, IPCC, 2021: climate Change 2021: the Physical Science Basis, Contribution of Working Group I to the Sixth Assessment Report of the Intergovernmental Panel on Climate Change (2021). https://www.ipcc.ch/report/ar6/wg1/#FullReport.

[2] P. Hewlett, M. Liska, F.M. Lea, Lea's Chemistry of Cement and Concrete, 5th ed., Butterworth-Heinemann, Oxford, 2019.

[3] Á.G.de La Torre, A.J.M. Cuberos, G. Álvarez-Pinazo, A. Cuesta, M.A.G. Aranda, In Situ Powder Diffraction Study of Belite Sulfoaluminate Clinkering, Urn:Issn:0909-0495. 18 (2011) 506–514. https://doi.org/10.1107/S0909049511005796.

[4] T. Hanein, A. Elhoweris, I. Galan, F.P. Glasser, M.N.C. Bannerman, Thermodynamic data of ye'elemite (C4A3S̄) for cement clinker equilibrium calculations, (2015). https://abdn.pure.elsevier.com/en/publications/thermodynamic-data-of-yeelemite-c4a3s-for-cement-clinker-equilibr (accessed March 31, 2021).

[5] S. Telschow, Clinker Burning Kinetics and Mechanism, Technical University of Denmark, 2012. https://orbit.dtu.dk/en/publications/clinker-burning-kinetics-and-mechanism. accessed February 25, 2021.

[6] T.T. Tran, Fluoride Mineralization of Portland Cement: Applications of Double-resonance NMR Spectroscopy in Structural Investigations of Guest Ions in Cement Phases, Interdisciplinary Nanoscience Center, Aarhus University, Aarhus, 2011. PhD Thesis.

[7] D. Herfort, G.K. Moir, V. Johansen, F. Sorrentino, H.B. Arceo, The chemistry of Portland cement clinker, Adv. Cement Res. 22 (2010) 187–194, https://doi.org/10.1680/adcr.2010.22.4.187.

[8] E.G. Shame, F.P. Glasser, Stable Ca3SiO5 solid solutions containing fluorine and aluminium made between 1050 and 1250 C, British Ceramic. Transactions and Journal 86 (1987) 13–17.

[9] V. Isteri, K. Ohenoja, T. Hanein, H. Kinoshita, M. Illikainen, P. Tanskanen, T. Fabritius, The Effect of Fluoride and Iron Content on the Clinkering of Alite-Ye'elimite-Ferrite (AYF) Cement Systems, Front Built Environ 7 (2021) 89, https://doi.org/10.3389/FBUIL.2021.698830/BIBTEX.

[10] T. Hanein, T.Y. Duvallet, R.B. Jewell, A.E. Oberlink, T.L. Robl, Y. Zhou, F. P. Glasser, M.N. Bannerman, Alite calcium sulfoaluminate cement: chemistry and thermodynamics, Adv. Cement Res. 31 (2019) 94–105, https://doi.org/10.1680/jadcr.18.00118.

[11] J.D. Zea-Garcia, I. Santacruz, M.A.G. Aranda, A.G. de la Torre, Alite-belite-ye'elimite cements: effect of dopants on the clinker phase composition and properties, Cem. Concr. Res. 115 (2019) 192–202, https://doi.org/10.1016/j.cemconres.2018.10.019.

[12] T. Duvallet, Influence of Ferrite Phase in Alite-Calcium Sulfoaluminate Cements, University of Kentucky University of Kentucky, 2014. PhD dissertation, https://uknowledge.uky.edu/cme_etds/27. accessed February 25, 2021.

[13] Y. Hu, W. Li, S. Ma, Q. Wang, H. Zou, X. Shen, The composition and performance of alite-ye'elimite clinker produced at 1300 °C, Cem. Concr. Res. 107 (2018) 41–48, https://doi.org/10.1016/J.CEMCONRES.2018.02.009.

[14] D. Adolfsson, N. Menad, E. Viggh, B. Björkman, Steelmaking slags as raw material for sulphoaluminate belite cement, 19 (2015) 147–156. https://doi.org/10.1680/ADCR.2007.19.4.147.

[15] V. Isteri, K. Ohenoja, T. Hanein, H. Kinoshita, P. Tanskanen, M. Illikainen, T. Fabritius, Production and properties of ferrite-rich CSAB cement from metallurgical industry residues, Sci. Total Environ. 712 (2020) 136208, https://doi.org/10.1016/j.scitotenv.2019.136208.

[16] R.I. Iacobescu, G.N. Angelopoulos, P.T. Jones, B. Blanpain, Y. Pontikes, Ladle metallurgy stainless steel slag as a raw material in Ordinary Portland Cement production: a possibility for industrial symbiosis, J. Clean. Prod. 112 (2016) 872–881, https://doi.org/10.1016/J.JCLEPRO.2015.06.006.

[17] M.T. Blanco-Varela, A. Palomo, F. Puertas, T. Vázquez, Influence of the joint incorporation of CaF2 and CaSO4 in the clinkerization process. Obtainment of new cements, Materiales de Construcción 45 (1995) 21–39, https://doi.org/10.3989/mc.1995.v45.i239.551.

[18] N. Chitvoranund, F. Winnefeld, C.W. Hargis, S. Sinthupinyo, B. Lothenbach, Synthesis and hydration of alite-calcium sulfoaluminate cement, Adv. Cement Res. 29 (2017) 101–111, https://doi.org/10.1680/jadcr.16.00071.

[19] D. Londono-Zuluaga, J.I. Tobón, M.A.G. Aranda, I. Santacruz, A.G. de la Torre, Clinkering and hydration of belite-alite-yeelimite cement, Cem. Concr. Compos. 80 (2017) 333–341, https://doi.org/10.1016/j.cemconcomp.2017.04.002.

[20] H. Shen, E. Forssberg, U. Nordström, Physicochemical and mineralogical properties of stainless steel slags oriented to metal recovery, Resour. Conserv. Recycl. 40 (2004) 245–271, https://doi.org/10.1016/S0921-3449(03)00072-7.

[21] D. Durinck, S. Arnout, G. Mertens, E. Boydens, P.T. Jones, J. Elsen, B. Blanpain, P. Wollants, Borate Distribution in Stabilized Stainless-Steel Slag, J. Am. Ceram. Soc. 91 (2008) 548–554, https://doi.org/10.1111/J.1551-2916.2007.02147.X.

[22] G. Adegoloye, A.L. Beaucour, S. Ortola, A. Noumowé, Concretes made of EAF slag and AOD slag aggregates from stainless steel process: mechanical properties and durability, Constr. Build. Mater. 76 (2015) 313–321, https://doi.org/10.1016/J.CONBUILDMAT.2014.12.007.

[23] R.M. Santos, T. van Gerven, Process intensification routes for mineral carbonation*, Greenhouse Gases: Sci. Technol. 1 (2011) 287–293, https://doi.org/10.1002/GHG.36.

[24] J.J. Beaumont, R.M. Sedman, S.D. Reynolds, C.D. Sherman, L.H. Li, R.A. Howd, M. S. Sandy, L. Zeise, G.v. Alexeeff, Cancer mortality in a Chinese population exposed to hexavalent chromium in drinking water, Epidemiology 19 (2008) 12–23, https://doi.org/10.1097/EDE.0B013E31815CEA4C.

[25] A. Seki, Y. Aso, M. Okubo, F. Sudo, K. Ishizaka, Development of Dusting Prevention Stabilizer for Stainless Steel Slag, (1986).

[26] A. di Maria, M. Salman, M. Dubois, K. van Acker, Life cycle assessment to evaluate the environmental performance of new construction material from stainless steel slag, The International Journal of Life Cycle Assessment 23 (2018) 2091–2109, https://doi.org/10.1007/S11367-018-1440-1, 2018 23:11.

[27] H. ming Wang, L. li Yang, G. rong Li, X. Zhu, H. Zhu, Y. tao Zhao, Effects of B2O3 and CaF2 on Melting Temperatures of CaO-SiO2-Fe2O3 System Fluxes, J. Iron and Steel Res., Int. 20 (2013) 21–24, https://doi.org/10.1016/S1006-706X(13)60106-5.

[28] E.D. Adesanya, A Cementitious binder from High-Alumina Slag Generated in the Steelmaking process, Doctoral Thesis, University Of Oulu, 2019.

[29] A. Adediran, J. Yliniemi, M. Illikainen, Mineralogy and glass content of Fe-rich fayalite slag size fractions and their effect on alkali activation and leaching of heavy metals, Int. J. Ceramic Eng. & Sci. 3 (2021) 287–300, https://doi.org/10.1002/CES2.10107.

[30] A.M. Rashad, Phosphogypsum as a construction material, J Clean Prod 166 (2017) 732–743, https://doi.org/10.1016/j.jclepro.2017.08.049.

[31] V. Isteri, K. Ohenoja, T. Hanein, H. Kinoshita, H. Kletti, C. Rößler, P. Tanskanen, M. Illikainen, T. Fabritius, Ferritic calcium sulfoaluminate belite cement from metallurgical industry residues and phosphogypsum: clinker production, scale-up, and microstructural characterisation, Cem. Concr. Res. 154 (2022) 106715, https://doi.org/10.1016/J.CEMCONRES.2022.106715.

[32] ISO 13320:2009, Particle size analysis — Laser diffraction methods, (2009). https://www.iso.org/standard/44929.html (accessed February 25, 2021).

[33] A. Cuesta, A.G. de La Torre, E.R. Losilla, V.K. Peterson, P. Rejmak, A. Ayuela, C. Frontera, M.A.G. Aranda, Structure, atomistic simulations, and phase transition of stoichiometric yeelimite, Chem. Mater. 25 (2013) 1680–1687, https://doi.org/10.1021/cm400129z.

[34] W.G. Mumme, Crystal structure of tricalcium silicate from a Portland cement clinker and its application to quantitative XRD analysis, Neues Jahrbuch Für Mineralogie-Monatshefte 1995 (1995) 146–160.

[35] W.G. Mumme, R.J. Hill, G. Bushnell-Wye, E.R. Segnit, Rietveld crystal structure refinements, crystal chemistry and calculated powder diffraction data for the polymorphs of dicalcium silicate and related phases, Neues Jahrbuch Fuer Mineralogie - Abhandlungen 169 (1995) 35–68.

[36] G.J. Redhammer, G. Tippelt, G. Roth, G. Amthauer, Structural variations in the brownmillerite series Ca2(Fe2-xAlx)O5: single-crystal X-ray diffraction at 25 °C and high-temperature X-ray powder diffraction (25 °C ≤ T ≤ 1000 °C), Am. Mineral. 89 (2004) 405–420, https://doi.org/10.2138/am-2004-2-322.

[37] L. Palacios, A. Cabeza, S. Bruque, S. García-Granda, M.A.G. Aranda, Structure and electrons in mayenite electrides, Inorg. Chem. 47 (2008) 2661–2667, https://doi.org/10.1021/ic7021193.

[38] V.G. Tsirelson, A.S. Avilov, Y.A. Abramov, E.L. Belokoneva, R. Kitaneh, D. Feil, X-ray and Electron Diffraction Study of MgO, Acta Crystallogr. B. 54 (1998) 8–17, https://doi.org/10.1107/S0108768197008963.

[39] M. Merlini, M. Gemmi, G. Cruciani, G. Artioli, High-temperature behaviour of melilite: in situ X-ray diffraction study of gehlenite-kermanite-Na melilite solid solution, Phys. Chem. Miner. 35 (2008) 147–155, https://doi.org/10.1007/s00269-007-0206-2.

[40] I. Pajares, Á.G. de la Torre, S. Martínez-Ramírez, F. Puertas, M.-T. Blanco-Varela, M.A.G. Aranda, Quantitative analysis of mineralized white Portland clinkers: the structure of Fluorellestadite, Powder Diffr. 17 (2002) 281–286, https://doi.org/10.1154/1.1505045.
[41] Y. Shen, J. Qian, J. Chai, Y. Fan, Calcium sulphoaluminate cements made with phosphogypsum: production issues and material properties, Cem. Concr. Compos. 48 (2014) 67–74, https://doi.org/10.1016/j.cemconcomp.2014.01.009.
[42] D. Redaoui, F. Sahnoune, M. Heraiz, A. Raghdi, Mechanism and kinetic parameters of the thermal decomposition of gibbsite Al(OH)3 by thermogravimetric analysis, Acta Phys. Pol. A 131 (2017) 562–565, https://doi.org/10.12693/APHYSPOLA.131.562.
[43] L. Trusilewicz, F. Fernández-Martínez, V. Rahhal, R. Talero, TEM and SAED characterization of metakaolin. pozzolanic activity, J. Am. Ceram. Soc. 95 (2012) 2989–2996, https://doi.org/10.1111/J.1551-2916.2012.05325.X.
[44] W.G. Mumme, R.J. Hill, G. Bushnell-Wye, E.R. Segnit, Rietveld crystal structure refinements, crystal chemistry and calculated powder diffraction data for the polymorphs of dicalcium silicate and related phases, (1995).
[45] A. Cuesta, Á.G. de La Torre, E.R. Losilla, I. Santacruz, M.A.G. Aranda, Pseudocubic crystal structure and phase transition in doped ye'elimite, Cryst. Growth Des. 14 (2014) 5158–5163, https://doi.org/10.1021/CG501290Q/SUPPL_FILE/CG501290Q_SI_002.CIF.
[46] D.N. Batchelder, R.O. Simmons, Lattice Constants and Thermal Expansivities of Silicon and of Calcium Fluoride between 6° and 322°K, J. Chem. Phys. 41 (2004) 2324, https://doi.org/10.1063/1.1726266.
[47] P.D. Brotherton, J.M. Epstein, M.W. Pryce, A.H. White, Crystal structure of 'calcium sulphosilicate', Ca5(SiO4)2SO4, Aust. J. Chem. 27 (1974) 657–660, https://doi.org/10.1071/CH9740657.
[48] Y. Takéuchi, F. Nishi, Crystal-chemical characterization of the 3CaO·Al2O3—Na2O solid-solution series, Z Kristallogr Cryst Mater 152 (1980) 259–308, https://doi.org/10.1524/ZKRI.1980.152.14.259.
[49] H. Morikawa, I. Minato, T. Tomita, S. Iwai, Anhydrite: a refinement, Acta Crystallogr. B. 31 (1975) 2164–2165, https://doi.org/10.1107/s0567740875007145.
[50] P. Norby, Synchrotron Powder Diffraction using Imaging Plates: crystal Structure Determination and Rietveld Refinement, J. Appl. Crystallogr. 30 (1997) 21–30, https://doi.org/10.1107/S0021889896009995.
[51] H.F. Kay, P.C. Bailey, IUCr, Structure and Properties of CaTiO3, Urn:Issn:0365-110X. 10 (1957) 219–226. https://doi.org/10.1107/S0365110X57000675.
[52] M.Z. Stout, P. Bayliss, Crystal structure of two ferrian ulvospinels from British Columbia, The Canadian Mineralogist 18 (1980) 339–341.
[53] H. Kabir, R.D. Hooton, N.J. Popoff, Evaluation of cement soundness using the ASTM C151 autoclave expansion test, Cem. Concr. Res. 136 (2020) 106159, https://doi.org/10.1016/j.cemconres.2020.106159.
[54] D. Herfort, D.E. Macphee, Components in Portland Cement Clinker and Their Phase Relationships, Lea's Chemistry of Cement and Concrete (2019) 57–86, https://doi.org/10.1016/B978-0-08-100773-0.00003-4.
[55] F. Bullerjahn, M. Zajac, M. ben Haha, K.L. Scrivener, Factors influencing the hydration kinetics of ye'elimite; effect of mayenite, Cem. Concr. Res. 116 (2019) 113–119, https://doi.org/10.1016/J.CEMCONRES.2018.10.026.
[56] Y. el Khessaimi, Y. el Hafiane, A. Smith, Effect of fineness and citric acid addition on the hydration of ye'elimite, Constr. Build. Mater. 258 (2020) 119686, https://doi.org/10.1016/J.CONBUILDMAT.2020.119686.
[57] C. Jun, C. Xin, L. Futian, L. Lingchao, T. Bing, Influence of fluorite on the Ba-bearing sulphoaluminate cement, Cem. Concr. Res. 31 (2001) 213–216, https://doi.org/10.1016/S0008-8846(00)00450-6.
[58] B. Liu, S. Wang, Y. Chen, C. Gong, L. Lu, Effect of waste gypsum on the setting and early mechanical properties of belite-C2.75B1.25A3$ cement, J. Therm. Anal. Calorim. 125 (2016) 75–83, https://doi.org/10.1007/s10973-016-5265-5.
[59] G.K. Moir, Improvements in the early strength properties of Portland cement, Trans. R. Soc. Lond. A, Royal Soc (1983) 127–138, https://doi.org/10.1098/rsta.1983.0072.
[60] J. Gálvez-Martos, A. Valente, M. Martínez-Fernández, J. Dufour, Eco-efficiency assessment of calcium sulfoaluminate clinker production, J. Ind. Ecol. 24 (2020) 695–706, https://doi.org/10.1111/jiec.12967.
[61] T.T. Tran, D. Herfort, H.J. Jakobsen, J. Skibsted, Site preferences of fluoride guest ions in the calcium silicate phases of portland cement from 29Si{19F} CP-REDOR NMR spectroscopy, J. Am. Chem. Soc. 131 (2009) 14170–14171, https://doi.org/10.1021/ja905223d.
[62] F. Bullerjahn, M. ben Haha, Mineralizer for calcium sulfoaluminate ternesite cements, European Patent (2016). Application: EP3109215A1.
[63] Y. Shen, X. Chen, J. Li, P. Wang, J. Qian, Preparation and Performance of Ternesite–Ye'elimite Cement, Materials 2022 15 (2022) 4369, https://doi.org/10.3390/MA15124369.
[64] Y. Shen, P. Wang, X. Chen, W. Zhang, J. Qian, Synthesis, characterisation and hydration of ternesite, Constr. Build. Mater. 270 (2021) 121392, https://doi.org/10.1016/J.CONBUILDMAT.2020.121392.